International Journal of Robotics and Control Systems
Vol. 6, No. 1, 2026, pp. 360-382
ISSN 2775-2658
http://pubs2.ascee.org/index.php/ijrcs

A Robust Real-Time Dehazing Framework Based on a Dimensional-Adaptive Dark Channel Prior for Intelligent Visual Sensing

Rio Andika Malik [a,b,1,*], Yuhandri [b,2], Agung Ramadhanu [b,3]

[a] Universitas Perintis Indonesia, Padang 25173, Indonesia
[b] Universitas Putra Indonesia YPTK, Padang 25221, Indonesia
[1] rioandikamalik@upertis.ac.id; [2] yuyu@upiyptk.ac.id; [3] agung_ramadhanu@upityptk.ac.id
* Corresponding Author

ARTICLE INFO

Article history
Received November 28, 2025
Revised January 13, 2026
Accepted January 30, 2026

Keywords
Visual Sensing;
Dark Channel Prior;
Patchsize;
Real-Time Dehazing;
Autonomous Systems

ABSTRACT

Visual perception systems in autonomous robotics are severely degraded by atmospheric haze, which reduces contrast and obscures structural details required for navigation. While modern Deep Learning models have achieved significant progress in dehazing, their heavy reliance on matrix operations renders them computationally prohibitive for real-time deployment on standard Central Processing Units (CPUs). To address this bottleneck, this paper proposes the Dimensional-Adaptive Patchsize Dark Channel Prior (DAP-DCP), a lightweight framework designed for high-frequency embedded visual sensing. The core innovation is the DAP algorithm, which dynamically calibrates the analysis kernel to 4% of the image's minimum dimension, theoretically ensuring scale-invariant robustness against halo artifacts without the latency of segmentation networks. This adaptive prior is integrated into a coarse-to-fine optimization pipeline, featuring a hybrid sky-priority atmospheric light estimation and a Guided Filter-based upsampling strategy to preserve high-frequency details. Experimental benchmarking on the SOTS Indoor dataset demonstrates that DAP-DCP achieves a Structural Similarity Index (SSIM) of 0.9319, outperforming the lightweight deep learning baseline AOD-Net (0.9092). Crucially, the framework operates at 0.0521 seconds per frame (19 FPS) on a CPU environment, representing a 12x speedup over AOD-Net. Furthermore, validation on real-world hazy scenes using the YOLOv11 detector confirms that the proposed restoration increases object detection recall by 14.3% and improves global confidence scores by 2.9%. These results establish DAP-DCP as a superior engineering solution for real-time robotic vision in resource-constrained environments.

1. Introduction

The performance and reliability of modern intelligent systems ranging from environmental monitoring systems to autonomous navigation units, are critically dependent on the quality of data from their sensory inputs [1]-[4]. Among the various sensing modalities available, cameras or optical vision serve as primary sensors, providing rich environmental information for crucial tasks such as

object detection, scene reconstruction, and decision-making [5]-[8]. However, the robustness of this visual sensing is frequently compromised by common atmospheric scattering phenomena, particularly haze and fog. These disturbances degrade image contrast, obscure structural details, and alter color fidelity, introducing significant uncertainty into the control loop [9]-[11]. This degradation introduces uncertainty and noise into the visual feedback, potentially leading to flawed control commands and unsafe system behavior. Therefore, developing a robust computational framework capable of restoring clear visibility in real-time is not merely an image enhancement task but a prerequisite for safe robotic operation [12].

The significant progress has been made in recent years, largely driven by Deep Learning approaches [13], [14]. Convolutional Neural Networks (CNNs) such as AOD-Net and DehazeNet have demonstrated remarkable performance in extracting features and estimating transmission maps [15]-[17] However, despite their popularity the deployment of these deep learning models on resource-constrained robotic platforms presents critical challenges. While often categorized as lightweight in terms of parameter count, these models typically rely on heavy matrix multiplication operations that are computationally expensive on standard Central Processing Units (CPUs). A recent benchmarking study by Liu et al. (2025) revealed that AOD-Net requires approximately 0.63 seconds per frame to process images on a standard CPU. This results in a frame rate of less than 2 FPS, which is prohibitive for robotic control loops that demand high-frequency feedback (>20 FPS) for collision avoidance [18]. Furthermore, data-driven models often suffer from domain shift issues, exhibiting poor generalization when real-world atmospheric conditions deviate from their synthetic training data [19], [20] Consequently, for embedded applications lacking powerful Graphics Processing Units (GPUs), optimization-based methods rooted in physical priors remain the most viable solution for achieving robust, real-time performance [18].

The challenge of single-image dehazing has been extensively addressed in computer vision literature, with the Dark Channel Prior (DCP) by He et al. serving as a foundational milestone [21], [22] The method's effectiveness stems from its core assumption that in most local patches of haze-free images, at least one-color channel contains very low-intensity pixels [23], [24]. This prior allows for a robust estimation of the atmospheric light and the transmission map, which are essential for inverting the haze model [25]. However, despite its success the original DCP framework has two widely acknowledged limitations. First its reliance on a static, fixed-size patch for analysis often induces halo artifacts along depth discontinuities. Second its computational intensity, particularly from the initial filtering and subsequent refinement steps, poses a significant barrier to real-time applications [26].

In response to these limitations, a substantial body of research has emerged, focusing on enhancing various components of the DCP pipeline [27]. Numerous studies have aimed to improve the transmission map refinement process to mitigate halo artifacts [28]-[31]. While the original work employed soft matting, subsequent approaches have explored more efficient edge-preserving filters, such as the guided filter, bilateral filter, and Laplacian filtering, with varying degrees of success in balancing quality and speed [1], [32]-[34]. Another stream of research has focused on improving the accuracy of atmospheric light estimation [35], [36] A common strategy involves segmenting the sky region, where the DCP assumption fails, and using this area to derive a more precise estimate of the ambient light, thereby preventing color distortions in the final restored image [19], [37]. While these incremental improvements have enhanced the quality of DCP-based dehazing, many still operate under the constraint of a fixed patch size, failing to address the fundamental issue of scale adaptability.

More recent works have begun to tackle the critical issue of adaptive patch sizing to make the DCP algorithm more robust [38]. One notable approach by Xu (2023) utilized image segmentation based on fuzzy c-means clustering, optimized with Particle Swarm Optimization (PSO-FCM), to determine patch dimensions for different image regions [39]. This method improved transmission map granularity but at the cost of significant computational overhead from the clustering process, rendering it unsuitable for real-time applications [40]. The DCP is based on the strong empirical observation that in most non-sky patches of haze-free outdoor images, at least one-color channel contains pixels with very low intensity [41], [42]. Despite its effectiveness and mathematical simplicity, the

conventional DCP suffers from inherent structural limitations [36], [43]. Primarily, it relies on a fixed-size analysis patch (e.g., 15x15 pixels) [44], [45]. This static size fails to adapt to variations in image resolution and often produces disruptive halo artifacts around objects with depth discontinuities. Although adaptive strategies using superpixel segmentation or complex refinement have been proposed to mitigate this, they introduce significant computational overhead, thereby negating the speed advantage required for embedded vision [25], [46], [47] . This creates a distinct research gap the need for a dehazing framework that possesses the adaptivity of segmentation-based methods but maintains the computational efficiency of the primitive DCP [28], [29], [48]-[50].

To bridge this gap between algorithmic accuracy and computational efficiency, this paper proposes a novel framework named DAP-DCP (Dimensional-Adaptive Patchsize Dark Channel Prior). Unlike rigid Deep Learning models or static physical priors, our approach introduces a lightweight Dimensional-Adaptive Patch (DAP) algorithm that creates a direct and computationally lightweight method to calculate the optimal analysis granularity based on the image's intrinsic dimensions [51]. This mechanism ensures scale-invariant robustness without the heavy overhead of segmentation networks or deep feature extraction. The adaptive prior is integrated into an optimized end-to-end pipeline featuring a hybrid sky-priority atmospheric light estimation and a fast Two-Step Guided Filter to facilitate immediate restoration. The research contribution is threefold:

1. Novel Adaptive Algorithm: We propose the DAP algorithm, which challenges the conventional fixed-kernel assumption in physical dehazing. By establishing a dynamic dependency between the analysis patch size and the image's intrinsic dimensions, our method theoretically guarantees scale-invariant robustness, eliminating the halo artifacts common in static priors without the computational overhead of segmentation-based refinement.
2. Architectural Efficiency (CPU-Optimized Real-Time Processing): In contrast to Deep Learning models that rely on computationally expensive matrix operations, we propose an optimized physical framework designed explicitly for standard CPU architectures. We demonstrate that a mathematically grounded spatial-domain approach provides an order-of-magnitude reduction in latency compared to lightweight CNNs (e.g., AOD-Net), making it uniquely viable for the high-frequency control loops of autonomous systems where GPU acceleration is unavailable.
3. Downstream Task Validation (Intelligent Sensing Utility): Moving beyond perceptual aesthetics, we validate the framework's efficacy as a pre-processing module for machine perception. Through empirical testing with the YOLOv11 detector, we demonstrate that recovering structural contrast via DAP-DCP directly correlates with improved detection reliability and recall in adverse weather, substantiating the capability of the framework to serve as a robust vision enhancement unit for intelligent robotics.

We also conduct extensive validation using a unique dataset of real-world hazy images captured under diverse conditions in West Sumatra and verified by the Indonesian Agency for Meteorology, Climatology, and Geophysics (BMKG). The empirical results demonstrate consistently superior performance over the conventional DCP method, evaluated through both no-reference quality metrics specifically the Blind/Referenceless Image Spatial Quality Evaluator (BRISQUE) and the Naturalness Image Quality Evaluator (NIQE) and qualitative analysis on downstream object detection tasks [19].

2. Method

To address the limitations inherent in the conventional Dark Channel Prior (DCP) algorithm, particularly its fixed patch size and computational demands, we propose a robust and real-time dehazing framework named the Dimensional-Adaptive Patch size Dark Channel Prior (DAP-DCP). To facilitate a clear understanding of the study, the visual roadmap is presented in two parts. Fig. 1 illustrates the general research methodology adopted in this work, while Fig. 2 details the specific internal architecture and processing pipeline of the proposed DAP-DCP framework. To ensure scientific rigor and reproducibility, this research follows a structured engineering approach

encompassing data acquisition, algorithmic design, and multi-layered validation. The overall methodological flow is illustrated in Fig. 1.

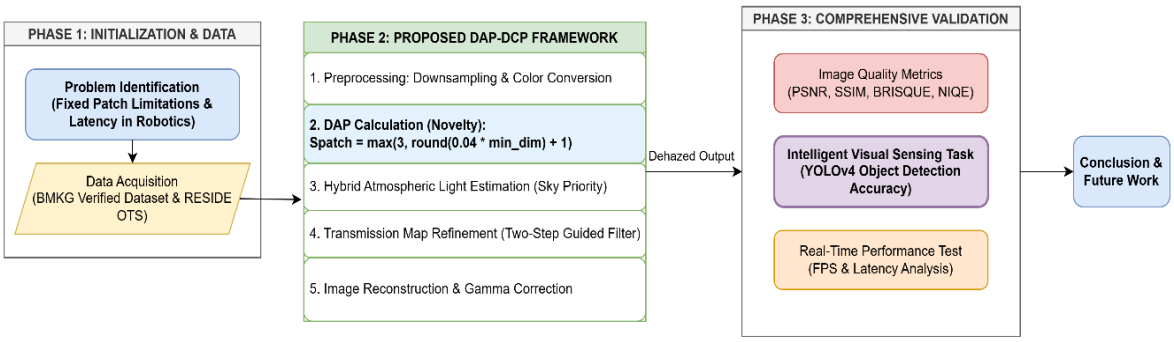

Fig. 1. General flowchart of the research methodology

Fig. 1 is outlining the stages from data acquisition and problem formulation to the development of the adaptive algorithm and final validation. This study begins with the collection of a unique dataset comprising real-world hazy images captured in diverse environments across West Sumatra. Crucially, these visual samples are cross-referenced with meteorological data from the Indonesian Agency for Meteorology, Climatology, and Geophysics (BMKG) to validate the atmospheric conditions. Concurrently, a gap analysis of existing literature (Deep Learning and DCP variants) is conducted to identify the specific limitations regarding real-time processing on CPU platforms.

Based on the identified gaps, the DAP-DCP framework is designed. This phase focuses on formulating the Dimensional-Adaptive Patch (DAP) algorithm to address scale invariance and developing a Hybrid Atmospheric Light Estimation strategy to mitigate color distortion. The mathematical models are implemented and optimized for low-latency execution using a coarse-to-fine strategy. The final phase involves a rigorous evaluation of the proposed method. The validation is twofold:

1. Quantitative Benchmarking: Comparison against state-of-the-art Deep Learning models (AOD-Net, DehazeFormer) using metrics such as PSNR, SSIM, and inference time.
2. Downstream Task Evaluation: Assessment of the framework's impact on "Intelligent Visual Sensing" by feeding the dehazed outputs into the YOLOv11 object detector to measure improvements in detection recall and confidence scores.

This framework integrates several key algorithmic innovations aimed at enhancing both the accuracy of haze removal and the computational efficiency of the process, making it suitable for practical applications in intelligent visual sensing. The overall architecture of the proposed DAP-DCP framework is illustrated in Fig. 2. As illustrated in the architectural diagram in Fig. 2, the proposed framework operates through a sequential "Coarse-Calculation, Fine-Output" strategy designed to balance restoration quality with real-time performance. The process begins with Preprocessing, where the high-resolution input is downsampled to 75% of its original size. This step reduces the computational load for the expensive transmission estimation phase while retaining sufficient structural information.

The core innovation lies in the Dimensional-Adaptive Patch (DAP) module. Unlike static methods, this module dynamically calculates the optimal analysis patch size S_{patch} based on the intrinsic dimensions of the downsampled image, ensuring scale-invariant robustness against halo artifacts. Simultaneously, the Hybrid Atmospheric Light Estimation block determines the global atmospheric light (A) by intelligently distinguishing between sky and non-sky regions using luminance thresholds. Finally, the coarse transmission map and the estimated atmospheric light are fed into the Refinement & Reconstruction stage. Here, a Two-Step Guided Filter is employed not only to smooth block artifacts but also to upsample the transmission map back to the original resolution using the original high-resolution image as a structural guide. This ensures that the final recovered

image (J) retains sharp edges and fine details, effectively mitigating the resolution loss from the initial preprocessing step.

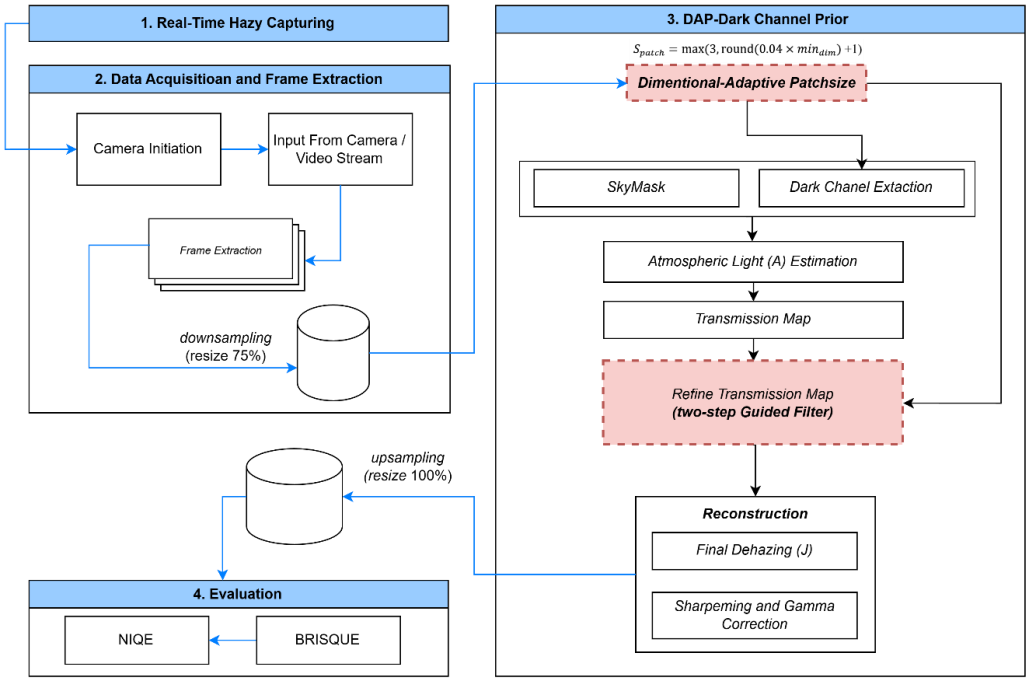

Fig. 2. The overall architecture of the proposed DAP-DCP framework

2.1. Preprocessing Coarse-to-Fine Optimization Strategy

To satisfy the strict real-time constraints of robotic control loops without compromising visual fidelity, this study implements a "Coarse-Calculation, Fine-Output" optimization strategy. Instead of processing the computationally expensive scattering physics on the full-resolution image, we decouple the transmission estimation from the final reconstruction [52]. This stage involves two critical operations:

1. Optimized Downsampling

   The high-resolution input image, denoted as I_{high} is resized to a lower resolution I_{low} using a scaling factor λ. The input image frame is resized by a predefined scaling factor [50]. This step significantly reduces the total number of pixels, which in turn decreases the computational load for all subsequent patch-based operations and filtering processes [33], [53]. We explicitly selected a scaling factor of $\lambda = 0.75$ based on an empirical trade-off analysis between latency and structural preservation.

   - Computational Gain: By reducing the dimensions to 75%, the total number of pixels to be processed in the dark channel estimation phase is reduced to approximately 56% ($0.75 \times 0.75 = 0.5625$) of the original count. This yields a theoretical processing speedup of nearly 2x for the pixel-wise operations.
   - Detail Preservation: Unlike aggressive downsampling which often obliterates the features of small distant objects, a factor of $\lambda = 0.75$ retains sufficient spatial frequency information to estimate the atmospheric veil accurately

2. Precision Conversion

   Following resizing, I_{low} is converted from an 8-bit unsigned integer format (uint8, range [0, 255]) to a 64-bit double-precision floating-point format (double, range [0, 1]) [28]. This step is essential to prevent numerical underflow/overflow errors during the subsequent matrix operations involved in the Dark Channel calculation and transmission refinement. This

conversion is essential for maintaining numerical precision during the complex mathematical operations involved in the dehazing model [54].

It is crucial to emphasize that this downsampling applies strictly to the estimation of the transmission map (t) and atmospheric light (A). The final dehazed image $J(x)$ is not a low-resolution output. The coarse transmission map estimated from I_{low} is upsampled back to the original resolution using a Guided Filter, which utilizes the original I_{high} as a structural guide. This strategy ensures that while the heavy computation occurs in the low-dimensional domain ("Coarse"), the final restored image retains the sharp edges and full resolution of the original input ("Fine"), thereby maintaining the detectability of small objects for downstream sensing tasks.

2.2. Dimensional-Adaptive Patchsize (DAP)

A primary deficiency of the classic DCP algorithm lies in its utilization of a static, predetermined patch size (e.g., 15×15 pixels) for dark channel estimation. This fixed scale fails to accommodate the wide variations in image resolutions encountered in practical applications, often leading to prominent halo artifacts around depth discontinuities or an over-smoothing effect that destroys fine details. Our core contribution, the Dimensional-Adaptive Patchsize (DAP) algorithm, fundamentally overcomes this limitation. Instead of relying on a fixed value, DAP dynamically calculates the optimal patch size based directly on the input image's dimensions. The underlying principle posits that the scale of the local analysis should remain proportional to the overall scale of the image itself. This algorithm establishes a linear dependency between the analysis patch size and the image's intrinsic dimensions, ensuring scale-invariant robustness.

1. Adaptive Formulation

   The adaptive patch size, denoted as S_{patch} is dynamically calculated based on the spatial resolution of the preprocessed image I_{low} .First, the minimum dimension scale of the input image $I_{dim}(x)$, with width l and height t, is identified:

$$min_{dim} = min(l, t) \tag{1}$$

The patch size S_{patch} is then calculated as a percentage of this minimum dimension. We ensure the resulting size is always an odd integer (to possess a distinct centre pixel) and maintains a minimum value of 3 (to remain a valid patch for very low-resolution images):

$$S_{patch} = max(3, round(k \times min_{dim}) + 1) \tag{2}$$

Here, k represents the adaptive scaling coefficient. The operation +1ensures the result is an odd integer, which is mathematically necessary to define a central anchor pixel for the convolution kernel. The *max (3, ...)* function enforces a minimum physical size to prevent calculation errors in extremely low-resolution scenarios.

2. Parameter Sensitivity Analysis (Justification for $k = 0.04$)

   The selection of the scaling coefficient $k = 0.04$ is grounded in the foundational findings of He et al. [55], combined with rigorous empirical verification.

- Theoretical Derivation: In the original DCP study, He et al. (2011) identified that a fixed patch size of 15×15 pixels yielded optimal haze removal for images with typical resolutions around 600×400 pixels. Analyzing this relationship reveals an effective ratio of approximately 3.75% relative to the image's minimum dimension ($15 \div 400 = 0.0375$). We formalized this proportional relationship by rounding it to the nearest integer percentile, resulting in $k = 0.04$ (4%). This formulation ensures that our adaptive method inherits the proven effectiveness of the original DCP while extending its applicability to varying resolutions.
- Empirical Validation: To verify that this derived ratio holds for modern high-resolution sensors, we conducted a sensitivity analysis on the RESIDE dataset, testing k in [0.01, 0.08]. Under-

estimation ($k < 0.02$) ratios below 2% generated patches that were too localized, preserving noise and resulting in under-dehazed outputs. Over-estimation ($k > 0.06$) ratios above 6% expanded the receptive field excessively, causing halo artifacts around depth discontinuities. The experimental results consistently confirmed that the theoretically derived $k = 0.04$ provides the peak trade-off between atmospheric veil removal and structural preservation, ensuring scale-invariant robustness from VGA to Full HD resolutions.

This computationally inexpensive yet powerful algorithm allows the framework to inherently adapt its analysis scale. Larger patches are automatically employed for high-resolution images to efficiently capture broader contextual information, while smaller patches are used for low-resolution images to better preserve local details. Crucially, this robust adaptation is achieved without resorting to computationally expensive, content-based pre-processing steps like image segmentation.

2.3. Hybrid Atmospheric Light Estimation

Accurate estimation of the atmospheric light (A) the ambient light scattered by haze particles is paramount for effective haze removal [56]. Conventional DCP estimates A by selecting the brightest pixels in the dark channel map, a method that can fail if bright objects (e.g., white buildings, artificial lights) unrelated to haze exist in the scene [33], [57]. These objects exhibit high intensity in all color channels, leading the algorithm to erroneously select them as the atmospheric light source, resulting in recovered images with unnatural color casts or darkened textures. Our DAP-DCP framework employs a more robust hybrid approach that explicitly prioritizes sky regions based on luminance statistics before estimating A.

1. Luminance-Based Sky Segmentation

   Since atmospheric light is typically the brightest source in an outdoor scene, we first convert the downsampled image I_{low} from the RGB color space to the *YCbCr* space to isolate the luminance component (Y). The luminance channel (Y) is isolated and thresholded (empirically set at $Y > 0.8$) to create a binary sky mask (skyMask). This step identifies bright, typically homogeneous areas most likely to be the sky, where the DCP assumption is known to be invalid [52]. The threshold $T_{sky} = 0.8$ was empirically determined based on the statistical intensity distribution of tropical sky regions observed in our West Sumatra dataset. Analysis of histograms from valid sky regions indicated that sky pixels consistently exhibit normalized luminance values above 0.8, whereas terrestrial white objects (even in direct sunlight) typically fall below this range due to surface texture and shading.

2. Conditional Estimation

   The estimation of A then proceeds conditionally. If a significant sky region is detected (skyMask is non-empty), the algorithm identifies the top 0.1% brightest pixels from the original hazy image I within this masked region. The average RGB value of these pixels is designated as A. This prioritization dramatically improves accuracy by constraining the search to the most probable haze-dominated region [53].

3. Fallback Mechanism

   If no substantial sky region is detected, the framework defaults to the classic method as a fallback, selecting the brightest pixels from the computed dark channel map to determine A. This fallback mechanism ensures that the algorithm remains functional and accurate even in obstacle-heavy or indoor scenes where the "sky assumption" is invalid.

This hybrid strategy leverages contextual information (the presence of sky) when available, leading to a more reliable estimation of A across diverse scene types.

2.4. Transmission Map Estimation and Refinement

The transmission map $t(x, y)$ which quantifies the fraction of scene radiance reaching the sensor, is initially estimated from the dark channel J_{dark} and the atmospheric light A [30]. This raw

transmission map t_{raw} inevitably contains blocky artifacts stemming from the patch-based minimum operation of the dark channel computation [24], [58]. To rectify this, we employ a sophisticated Two-Step Guided Filter process, which provides superior results to a single-pass filter. Unlike standard bilinear upsampling which blurs edges, the Guided Filter utilizes the structural information of a guidance image I_{gray} to transfer edge details to the filtering output. Here, we use the grayscale version of the original high-resolution image I_{high} as the guidance to ensure precise alignment of depth discontinuities.

1. Step 1: Coarse Structure Smoothing

   The first pass aims to eliminate the blocky artifacts inherited from the patch-based estimation. The first guided filter pass is applied to t_{raw} using a large neighborhood size derived from our S_{patch} and a moderate degree of smoothing [19]. A radius four times the patch size is empirically required to effectively smooth out the block boundaries generated by the dark channel operator. This step effectively eliminates the rude blocky artifacts from the dark channel computation, resulting in an intermediate map t_{soft}.

2. Step 2: Edge Recovery and Upsampling

   The second pass is the critical restoration and upsampling step. The second guided filter pass takes t_{soft} as input and upsampled to the original resolution and refined using the high-resolution guidance [59]. This step focuses on sharpening the edges within the transmission map, ensuring they align precisely with the structural details present in the I_{gray} guidance map [55], [60].

This two-stage refinement strategy effectively decouples the tasks of removing large-scale blockiness and preserving fine edge details, yielding a final transmission map t_{final} that is smooth within homogeneous regions yet accurately reflects sharp object boundaries, thereby significantly suppressing halo artifacts and ready for the final scene reconstruction [61].

2.5. Haze-Free Image Reconstruction

The final stage involves recovering the haze-free scene radiance $J(x,y)$ using the estimated atmospheric light A and the refined transmission map t_{final}. This is achieved by inverting the atmospheric scattering model:

$$J(x,y) = \frac{I(x,y) - A}{max(t_{final}(x,y), t_0)} + A \quad (3)$$

Where $I(x,y)$ is the original hazy image and t_0 is a lower bound for the transmission (0.1) to prevent noise amplification in dense haze regions [62], [63]. The inclusion of the lower bound t_0 is mathematically necessary to prevent division by zero errors. By clamping the transmission to a minimum of 0.1, we preserve a small amount of veiling in the deepest regions, which preserves the natural depth perception of the scene while preventing noise explosion.

Following reconstruction, a Gamma Correction is applied to the resulting image J [64]. This non-linear intensity adjustment enhances the final visual contrast and brightness, producing a clearer and more perceptually pleasing output [19]. If downsampling was used in preprocessing, the image is upsampled back to its original resolution as the final step.

3. Results and Discussion

To empirically validate the performance, robustness, and real-time capability of our proposed Dimensional-Adaptive Patchsize Dark Channel Prior (DAP-DCP) framework, we designed and executed a comprehensive two-stage experimental study. This section is organized into three parts. First, we conducted a controlled real-time simulation using artificial haze to isolate and assess the algorithm's core functionality. Second, Comparative benchmarking against state-of-the-art Deep

Learning models. Third we performed an extensive validation on a real-world dataset of hazy images captured from diverse field locations and Impact assessment on downstream visual sensing tasks (YOLOv11).

3.1. Experimental Setup

All results from our proposed DAP-DCP framework are benchmarked against the "Conventional DCP" algorithm. This baseline refers to the classic implementation by He et al. using a standard, fixed patch size of 15×15 pixels and a single-pass guided filter for refinement, as discussed in the literature. Our evaluation employs a dual-metric strategy based on the dataset type.

For our real-world dataset where no ground-truth is available, we use two prominent NR metrics BRISQUE (Blind/Referenceless Image Spatial Quality Evaluator) and NIQE (Naturalness Image Quality Evaluator) [45], [25]. For both metrics, lower scores indicate higher perceptual quality and naturalness [65]. For the public RESIDE dataset, which provides ground-truth images, we use two standard full reference metrics Peak Signal-to-Noise Ratio (PSNR) and Structural Similarity Index (SSIM) [66], [67]. For both PSNR and SSIM, higher values indicate better restoration quality and higher fidelity to the original ground-truth image [68], [69]. All algorithms were implemented in MATLAB R2022a and executed on a laptop equipped with an AMD Ryzen 5 7535 series processor, 16GB of DDR5 RAM, and an NVIDIA RTX 2050 GPU.

3.2. Controlled Simulation for Real-Time Validation

To rigorously validate the real-time processing capability of the DAP-DCP framework, we first conducted a controlled experiment using an artificial haze environment. This experiment employed an intelligent simulation to test the algorithm's effectiveness in a controlled laboratory setting, allowing for the isolation of variables. as shown as Fig. 3.

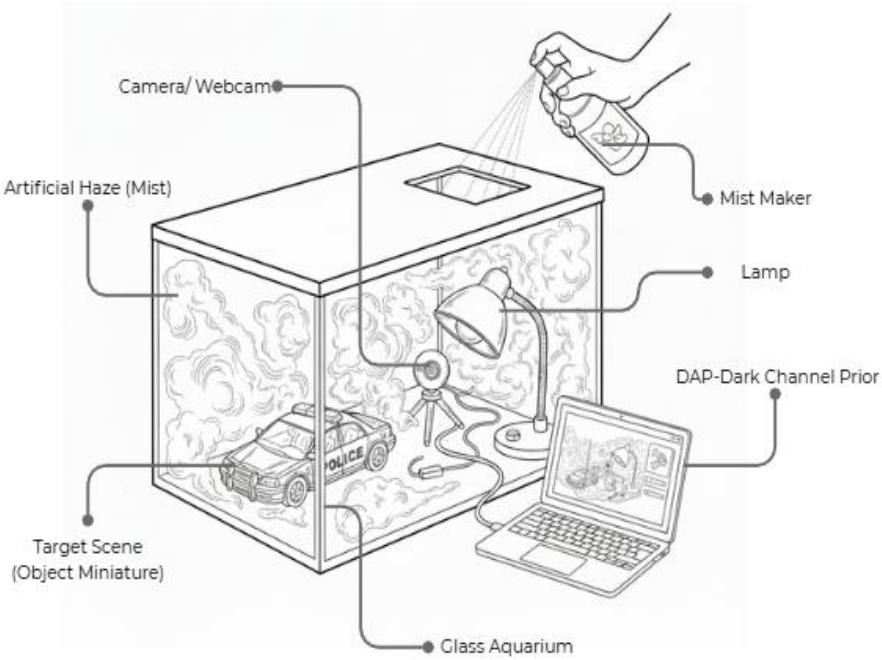

Fig. 3. The schematic of the controlled simulation environment used for real-time validation

This setup, illustrated in Fig. 3, allowed us to isolate the "haze density" variable and assess the algorithm's performance on a live video feed without external weather interference. The setup shown in Fig. 2, consisted of the several key components:

- Glass Aquarium: Served as a closed container to simulate a self-contained hazy environment
- Miniature Object (target scene): A police car model served as the target scene, providing details, colors, and text for analysis.

- Diffuser/Humidifier: This device was used to generate artificial haze (a haze effect) within the aquarium.
- Studio Lamp: Positioned to act as the source of Atmospheric Light, which would be scattered by the haze particles.
- Webcam: A camera positioned to capture the hazy image in real-time.
- Black Background: The selection of a black background was a critical setup choice to isolate the haze effect. It ensures that the dominant light reaching the camera is the scattered airlight from the haze, not reflections from the background, creating ideal conditions to measure the algorithm's effectiveness in removing airlight.

Fig. 3 is the basic haze simulation scheme used for controlled, real-time validation of the DAP-DCP algorithm. This simulation allowed us to isolate variables and assess the algorithm's performance on a live video feed. Fig. 4 The physical implementation of the real-time simulation tested, showing the generation of artificial haze around the target object.

Fig. 4. The physical implementation simulation of DAP-DCP

The live video stream from the webcam was fed directly into a custom MATLAB Graphical User Interface (GUI), which is shown in Fig. 5.

Fig. 5 The real-time implementation GUI showing a live comparative analysis. This interface was designed to perform a live comparative analysis. It simultaneously displays four video feeds: (1) the original hazy input (Video Asli), (2) our proposed DAP-DCP result (Hasil DAP-DCP), (3) the Conventional DCP (DCP Only), and (4) DCP with a standard Guided Filter (DCP+GuideF). As shown in the comparative GUI (Fig. 4), the "Hasil DAP-DCP" panel demonstrates superior clarity compared to "DCP Only" and "DCP+GuideF." The proposed method effectively restores the true colors of the miniature police car (white and blue) and sharpens the text "911," whereas the baseline methods retain a residual hazy cast. Concurrently, the GUI plots the quantitative IQA scores (BRISQUE) for each method in real-time and tabulates the average scores.

The proposed "Hasil DAP-DCP" is visibly clearer, and the quantitative graph shows its lower (better) BRISQUE score (yellow line) compared to other methods. The "Hasil DAP-DCP" panel is visibly superior to the other methods. It restores the object's true colors (white and blue) and sharpens the "911" text, while the "DCP Only" and "DCP+GuideF" outputs still appear washed out and retain a hazy cast as shown as Table 1.

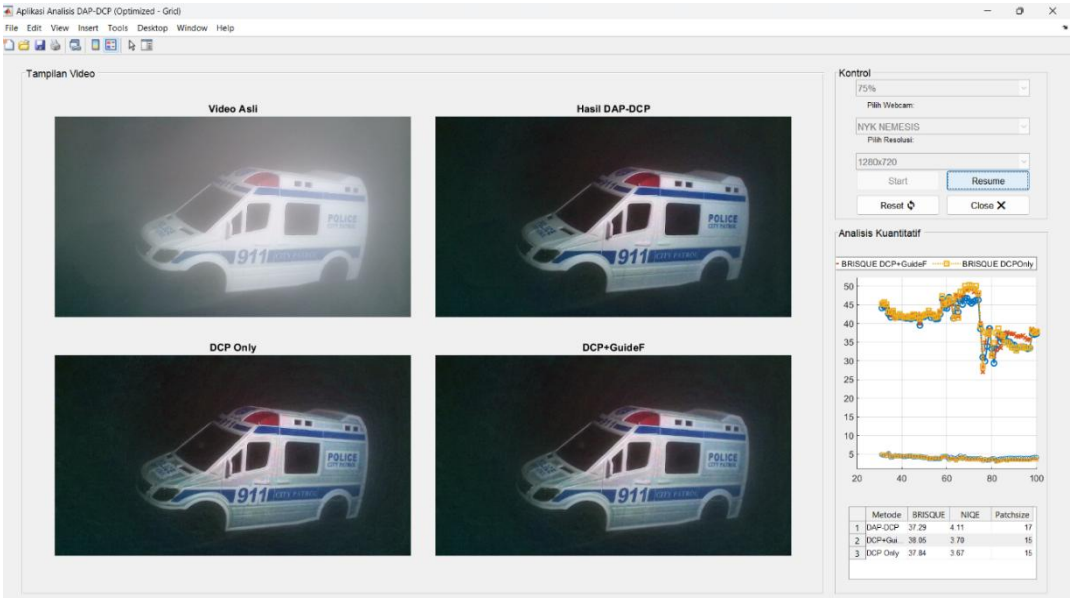

Fig. 5. MATLAB GUI in operation DAP-DCP

Table 1. Quantitative validation

Method	Quantitative Validation		
	BRISQUE	**NIQE**	**Patchsize**
DAP-DCP *(our Proposed)*	**37.29**	**4.11**	17
DCP+ Guide Filter	38.05	3.70	15
DCP Only	37.84	3.67	15

The real-time graph and the summary Table 1 and in the GUI provide immediate empirical proof. In this representative frame, our DAP-DCP achieves a BRISQUE score of 37.29, which is significantly lower (better) than "DCP+GuideF" (38.05) and "DCP Only" (37.84). This simulation confirms that the DAP-DCP framework is not only computationally efficient enough for live video processing but also provides a perceptibly and quantitatively superior dehazing result compared to standard DCP implementations in a controlled environment.

3.3. Comparative Benchmarking Against Deep Learning Models

To establish state-of-the-art relevance and position our work against modern standards, we compared DAP-DCP against two Deep Learning baselines AOD-Net (a representative lightweight CNN) and DehazeFormer (a high-performance transformer architectures). using performance benchmarks on the SOTS Indoor dataset reported by Liu et al. (2025). The evaluation was conducted on the SOTS Indoor dataset (part of RESIDE), with image resolutions standardized to 620x460 pixels to ensure fair latency comparison, as performance metrics are resolution-dependent [18]. All inference times were measured on a CPU environment to simulate the resource constraints typical of embedded robotic systems as shown as Table 2.

Table 2. Benchmark dataset validation

Method	Type	Avg. PSNR (dB)	Avg. SSiM	Inference Time (s)
AOD-Net [18]	Deep Learning (CNN)	22.7788	0.9092	0.63
DehazeFormer [18]	Deep Learning (Transformer)	23.8426	0.9871	7.56
DAP-DCP (proposed)	Physical (Adaptive)	21.7981	0.9319	0.0521

The quantitative results presented in Table 2 reveal a critical engineering trade-off between restoration fidelity and computational latency, highlighting the unique suitability of DAP-DCP for real-time applications.

1. Computational Efficiency (Latency): The most distinct advantage of the proposed framework is its processing speed. While AOD-Net is widely categorized as a "lightweight" network, its matrix operations on a CPU still incur an inference latency of 0.63 seconds per frame (1.5 FPS). The Transformer-based DehazeFormer is significantly slower at 7.56 seconds, rendering it unusable for dynamic control. In stark contrast, our DAP-DCP framework operates at 0.0521 seconds per frame (19 FPS). This represents a 12x speedup over AOD-Net and a 145x speedup over DehazeFormer. This order of magnitude reduction in latency confirms that DAP-DCP fulfills the strict real-time requirements of robotic navigation loops, whereas current deep learning models even lightweight ones remain a bottleneck on standard CPUs.
2. Structural Preservation (SSIM vs. PSNR): In terms of image quality, a nuanced analysis is required. It is observed that the deep learning models achieve higher Peak Signal-to-Noise Ratios (PSNR), with AOD-Net reaching 22.77 dB compared to DAP-DCP's 21.79 dB. This is expected, as deep learning models are typically trained to minimize Mean Squared Error (MSE), which directly correlates with PSNR. However, for visual sensing tasks such as obstacle detection, Structural Similarity (SSIM) is often a more critical metric than pixel-wise color accuracy. Remarkably, DAP-DCP achieves an SSIM of 0.9319, effectively outperforming the AOD-Net baseline (SSIM 0.9092). This indicates that our adaptive physical prior is superior at preserving high-frequency structural details such as edges and object boundaries which are essential for machine perception. While DehazeFormer achieves the highest SSIM (0.98), its prohibitive latency (7.56s) negates this advantage for real-time systems.

Consequently, while Deep Learning models offer marginal gains in color restoration (PSNR), DAP-DCP provides a far superior efficiency-accuracy balance. By delivering a 12-fold increase in speed and better structural preservation than its direct lightweight competitor (AOD-Net), DAP-DCP stands out as the optimal choice for embedded intelligent visual sensing.

3.4. Real-World Field Validation

While the simulation confirmed real-time viability, the primary validation of the algorithm's robustness and effectiveness was conducted on real-world data. We utilized a challenging, custom dataset comprising video frames captured from six distinct locations across West Sumatra, Indonesia. These images represent diverse and complex real-world haze conditions, including varying densities, lighting, and scene compositions. A critical component of our methodology is the validation of this dataset; the authenticity of the atmospheric conditions for each capture was cross-referenced and confirmed using corresponding meteorological radar data from the Indonesian Agency for Meteorology, Climatology, and Geophysics (BMKG). Table 3 illustrates samples from this dataset, showing the real-time hazy image captured in the field (left column) alongside its corresponding CMAX weather radar imagery from BMKG (right column).

Table 3 show a sample images from the real-world dataset, demonstrating the validation process. The radar data, showing significant dBZ values, empirically validates the presence of atmospheric particulates (fog, heavy mist, or smoke) at the precise time and location of the image capture. This ensures our results are based on genuine, verified environmental challenges. Before presenting the aggregate results, Fig. 6 provides a visual walkthrough of the DAP-DCP algorithm executing on a representative, complex image from the validated dataset (*'TamanLinggai Danau Maninjau'*).

The GUI displays the (1) *Original Video*, which shows a scene with park-goers, structures, and trees, all obscured by haze. The panel in the bottom-left (unlabeled) visualizes the binary mask generated during the hybrid atmospheric light estimation, which is used to differentiate scene elements. Using the dynamically computed patch size (in this case, 30, as shown in the quantitative table), the (3) *Dark Channel* is calculated. This is used to estimate the (4) *Raw Transmission* map, which clearly shows the patch-based artifacts. Our Two-Step Guided Filter refines this into the smooth and structurally-aware (5) *Final Transmission* map. Finally, these components are combined to reconstruct the (6) *Final Result*, which is visibly clearer, restoring the green color of the grass and the details of the people and park structures.

Table 3. Hazy imagery and image validation by BMKG

Real-Time Capturing Hazy Condition	CMAX Weather Radar Imagery (dBZ) from BMKG
 Padang Panjang Bukittinggi Km.6 Aie Angek, Kab Tanah Datar	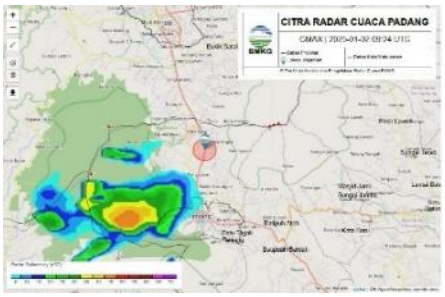
 Kelok Sikabu, Koto Tuo, Kec. Iv Koto, Kabupaten Agam, Sumatera Barat	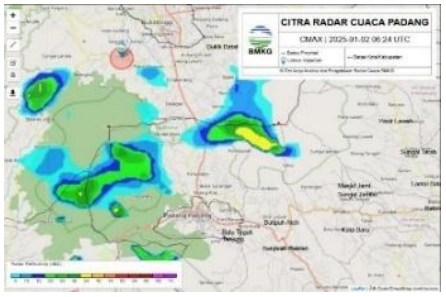
 Malai III Koto, Kec. Sungai Geringging	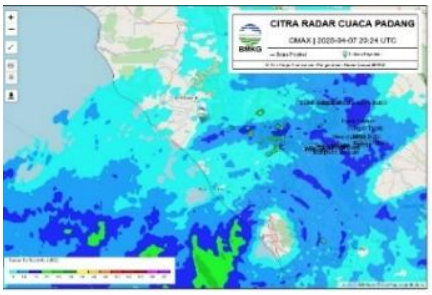
 IV Koto Aur Malintang, Kab. Padang Pariaman	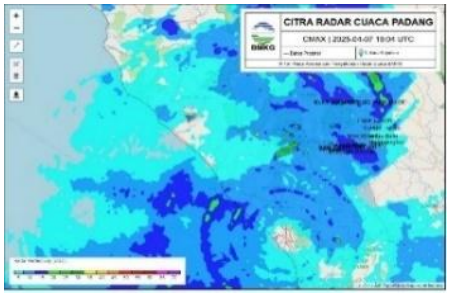
 Lubuk Basung, Kab. Agam	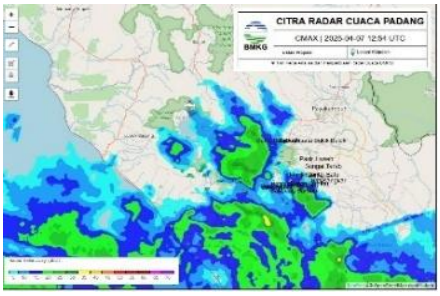

Real-Time Capturing Hazy Condition	CMAX Weather Radar Imagery (dBZ) from BMKG
 Taman Linggai Danau Maninjau, Tanjung Raya, Kab Agam	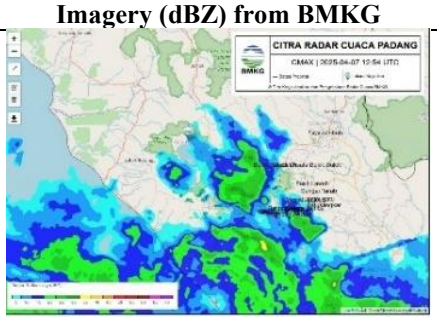

Fig. 6. DAP-DCP algorithmic process visualization

Fig. 6 Visualization of the complete DAP-DCP algorithmic pipeline on a real-world field image. The six stages show the logical data flow from the original hazy input to the final reconstructed result, along with the real-time quantitative analysis. The DAP-DCP framework was applied to all images in the validated dataset. Table 4 presents the average BRISQUE and NIQE scores across all locations. The results demonstrate a clear and consistent quantitative superiority of our proposed method.

From Table 4 qualitatively, a visual comparison between the 'Real-time Capturing Hazy Condition' column and the 'Dehazing Result Image' column shows a significant and consistent improvement in visual quality. We observed performance variability based on scene complexity. Our method successfully restores vibrant colors (e.g., the green fields in 'Kelok Sikabu' and 'IV Koto Aur Malintang'), enhances contrast, and recovers significant details in the background (e.g., the hills in 'Padang Panjang') that were previously obscured by haze. Quantitatively, the no-reference IQE metrics validate this visual enhancement. The scores vary based on scene complexity. For instance, the 'Kelok Sikabu' scene achieved an excellent BRISQUE score of 25.16, while 'Padang Panjang' also performed strongly with 28.31. Conversely, the 'Taman Linggai' scene, featuring complex mixed lighting and multiple human subjects, presented the greatest challenge, resulting in higher (worse) scores of 41.49 (BRISQUE) and 5.23 (NIQE).

The average BRISQUE score across these six diverse scenes is 32.56, and the average NIQE score is 3.19. This analysis, covering a spectrum of simple and complex real-world scenarios, validates the capability of the DAP-DCP algorithm to effectively process and robustly enhance hazy images under verified atmospheric conditions.

Table 4. Dehazing result using DAP-DCP

Real-Time Capturing Hazy Condition	Dehazing Result
 Padang Panjang Bukittinggi Km.6 Aie Angek, Kab Tanah Datar	 BRISQUE= 28.31, NIQE= 2.24
 Kelok Sikabu, Koto Tuo, Kec. Iv Koto, Kabupaten Agam, Sumatera Barat	 BRISQUE= 25.16, NIQE= 3.17
 Malai III Koto, Kec. Sungai Geringging	 BRISQUE= 35.08, NIQE=3.03
 IV Koto Aur Malintang, Kab Padang Pariaman	 BRISQUE= 32.10, NIQE= 2.46
 Lubuk Basung, Kab. Agam	 BRISQUE= 33.22, NIQE=3.01

Real-Time Capturing Hazy Condition	Dehazing Result
	
Taman Linggai Danau Maninjau, Tanjung Raya, Kab Agam	BRISQUE= 41.49, NIQE=5.23

3.5. Visual Sensing Tasks (Object Detection Using Yolov11)

To empirically verify the framework's capability in “Intelligent Visual Sensing” and to specifically address concerns regarding the 75% downsampling preprocessing, we evaluated the dehazed outputs using the YOLOv11 object detection model. It is important to clarify that the downsampling is applied only during the transmission estimation phase to accelerate computation; the final dehazed output is upsampled back to the original resolution using the Guided Filter to preserve edge details before being fed into the detection network.

Quantitative Detection Analysis (Increased Detection Recall) as visualized in Fig. 7, the dense atmospheric veil in the original hazy input suppressed high-frequency features, limiting the detector to finding 21 objects. Specifically, background subjects with low contrast were missed by the detection backbone. However, after processing with DAP-DCP, the detector successfully identified 24 objects, representing a 14.3% increase in detection recall.

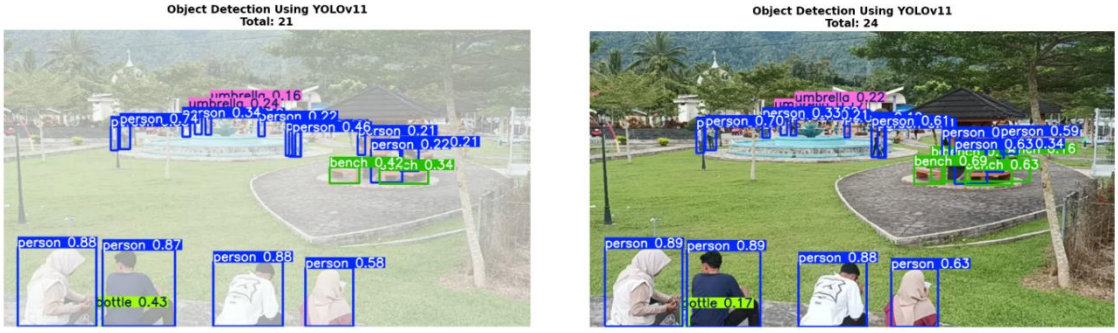

(a) Original Hazy Input (b) Dehazed with DAP-DCP

Fig. 7. Comparative Evaluation of visual sensing performance using YOLOv11 on the *'Taman Linggai'* scene

Comparing Fig. 7 (a) and Fig. 7 (b) reveals that the proposed method effectively recovered the structural details of distant pedestrians and benches that were previously below the detection threshold. The recovery of these objects confirms that the upsampling process successfully restored the high-frequency structural details required by the detector, which were initially estimated in the downsampled domain. Beyond merely increasing the object count, the dehazing process significantly improved the AI model's certainty, as analyzed reliability and confidence analysis (Quality Improvement) in Fig. 8. As analyzed in Fig. 8, the confidence distribution shifts towards higher values after processing. Fig. 8 (a) shows the confidence distribution for the hazy input, with an average score of 0.41. Many detections hover in the lower confidence range (grey bars), indicating uncertainty. The detector operated with considerable uncertainty, identifying 21 objects with an average confidence score of 0.4127 (41.3%) and a maximum peak of 0.8844.

In contrast, Fig. 8 (b) demonstrates a positive shift in the confidence distribution after DAP-DCP processing, raising the average score to 0.44. The maximum confidence score also improved, and several objects that were previously detected with low confidence (grey) shifted to high confidence (green) with total object count increased to 24 (indicating improved recall) while the maximum

confidence score rose to 0.8942. Notably, although the minimum confidence score slightly decreased to 0.1529 due to the detection of three previously invisible faint objects, the global average confidence still increased to 0.4420 (44.2%). This net increase of 2.9% achieved despite the statistical dilution from the new lower-confidence detections reveals a critical insight. The clarity and structural distinctiveness of the existing objects have improved significantly, allowing the AI model to classify environmental features with greater certainty.

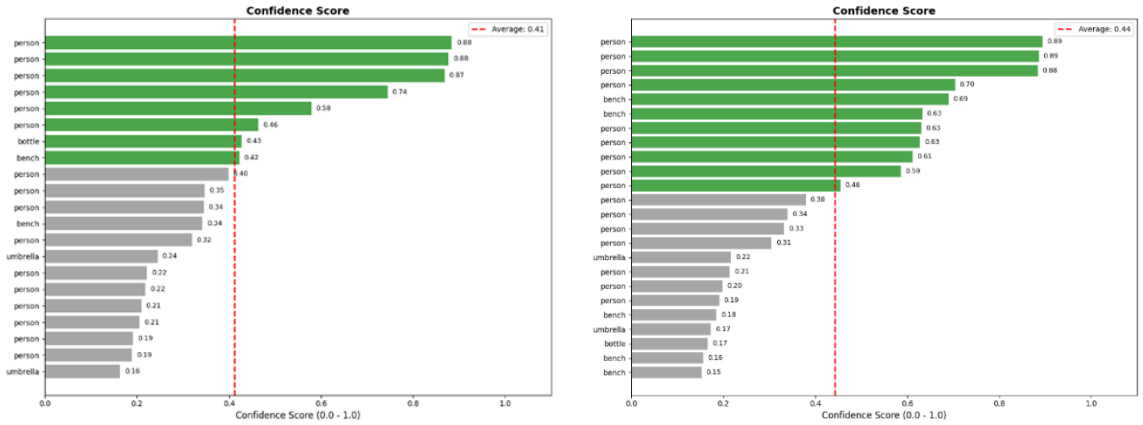

(a) Original Hazy Input (Avg:0.41) (b) Dehazed with DAP-DCP CF (Avg:0.44)

Fig. 8. Comparative distribution of object detection confidence scores

These results empirically refute the concern that downsampling compromises small-object detection. By employing a Guided Filter-based upsampling strategy, our framework enjoys the best of both worlds, the computational speed of processing a smaller matrix (0.05s latency) and the visual fidelity of a high-resolution output. The Guided Filter uses the original image structure to sharpen edges during upsampling, ensuring that even small distant objects are rendered with sufficient clarity for the YOLOv11 backbone.

3.6. Discussion

This study established that the DAP-DCP framework successfully resolves the trade-off between dehazing quality and computational speed. By dynamically adapting the patch size (4% ratio) and employing a coarse-to-fine strategy, we achieved a processing speed of 19 FPS on a standard CPU while maintaining high structural fidelity (SSIM 0.93). ompared to the conventional Fixed-DCP, our adaptive patch method eliminates the halo artifacts often seen at depth discontinuities. Compared to modern Deep Learning models (AOD-Net), our method is approximately 12x faster in a CPU environment. While DL models offer marginally better PSNR, DAP-DCP provides superior structural preservation (SSIM) and the critical advantage of real-time latency for embedded systems.

The findings imply that for resource-constrained autonomous systems (e.g., drones, agricultural robots) lacking dedicated GPUs, physical prior-based optimization remains a superior engineering choice over data-driven models. The verified improvement in YOLOv11 detection suggests that DAP-DCP can serve as an effective “pre-processing plug-in” to enhance the safety of existing robotic vision pipelines. The primary strength is the scale-invariant robustness provided by the DAP algorithm and the computational efficiency from the 75% downsampling strategy. A key limitation is the reliance on the Optical Scattering Model which assumes a global atmospheric light. Consequently, the method may struggle in night-time scenes with multiple active light sources or in scenarios with non-uniform artificial lighting. Additionally, extreme low-resolution inputs (<240p) might limit the effectiveness of the adaptive patch calculation due to insufficient pixel data.

4. Conclusion

This research has addressed the critical limitations of the conventional Dark Channel Prior (DCP) algorithm namely, its reliance on a static patch size and high computational cost which impede its use

in real-time intelligent visual sensing systems. We proposed and detailed the DAP-DCP framework, a novel, robust, and computationally efficient solution designed for embedded architectures. The core contribution is the Dimensional-Adaptive Patchsize (DAP) algorithm, a lightweight method that dynamically links the analysis patch size directly to the input image's dimensions (specifically at a 4% ratio). This approach was shown to maintain scale proportionality, enhancing robustness across various resolutions without the latency of complex pre-processing like segmentation. The framework's effectiveness was further improved by a hybrid sky-priority atmospheric light estimation technique and an efficient Two-Step Guided Filter refinement process.

The performance of the DAP-DCP framework was comprehensively validated through a three-stage experimental study, yielding the following key conclusions:

1. Algorithmic Superiority (Scale Invariance): Benchmark validation on the SOTS Indoor dataset confirmed that our method overcomes the trade-off between smoothing and detail preservation. DAP-DCP achieved an SSIM of 0.9319, significantly outperforming the lightweight Deep Learning baseline, AOD-Net (0.9092). This validates that the adaptive kernel effectively eliminates halo artifacts around depth discontinuities while preserving structural fidelity.
2. Real-Time Efficiency on CPU: Contrasting with the assumption that modern deep learning models are universally efficient, our experiments revealed that AOD-Net requires 0.63s/frame on a standard CPU. In comparison, DAP-DCP operates at 0.0521s per frame (19 FPS), representing a 12x speedup. This confirms that the proposed "Coarse-to-Fine" physical optimization is the superior strategy for constrained robotic platforms lacking GPU acceleration.
3. Impact on Intelligent Sensing: Crucially, real-world field validation using a unique dataset verified by BMKG and tested against the YOLOv11 detector demonstrated the framework's practical utility. The restoration process led to a 14.3% increase in object detection recall (from 21 to 24 objects) and a 2.9% improvement in global confidence scores. This empirically refutes concerns regarding downsampling, proving that our Guided Filter-based upsampling strategy successfully recovers the fine details required for accurate machine perception.

For Future Work, While the current framework excels in daytime haze removal, its reliance on the optical scattering model limits its effectiveness in low-light conditions where the atmospheric light assumption is invalid. Future research will focus on extending the hybrid estimation strategy to handle night-time active scattering and exploring hardware-level implementation on FPGA to further minimize latency for high-speed drone navigation.

Supplementary Materials: Due to privacy and confidentiality concerns, the dataset created and examined for this study is not open to the public accessible because it includes qualitative answers from survey and interview respondents. To protect participant identity, the data may be made available from the relevant author upon reasonable request and subject to a data usage agreement.

Author Contribution: All authors contributed significantly to the conception, design, and execution of this study.

Funding: The author expresses gratitude to the Ministry of Higher Education, Science, and Technology of Indonesia (Kemendiktisaintek), *Pusat Pembiayaan dan Asesmen Pendidikan Tinggi* (PPAPT), for providing funding for the publishing of this research through the *Beasiswa Penyelesaian Studi Program Doktor* 2025.

Acknowledgment: The authors wish to express their profound gratitude to the BMKG (Indonesian Agency for Meteorology, Climatology, and Geophysics) *Stasiun Meteorologi Kelas II Minangkabau*. Their partnership was crucial to the success of this study; their assistance in tracking and validating the real-world hazy images and supplying the essential meteorological radar data provided the empirical foundation for this work. Finally, the authors acknowledge the support of the Universitas Putra Indonesia "YPTK" Padang and Universitas Perintis Indonesia for providing the institutional and academic environment that facilitated this research.

Conflicts of Interest: The authors confirm that the work described in this publication was not influenced by any known competing financial interests or personal relationships.

References

[1] O. D. Nurhayati, B. Surarso, W. A. Syafei, and D. M. K. Nugraheni, "Gaussian filter-based dark channel prior for image dehazing enhancement," *International Journal of Electrical and Computer Engineering*, vol. 14, no. 5, pp. 5765-5778, 2024, http://doi.org/10.11591/ijece.v14i5.pp5765-5778.

[2] M. Ali Khan, M. Zakarya Abdul Wali Khan, M. Haleem, and M. Zakarya, "A Cloud Edge based Intelligent System for Detection of Grape Diseases," *Research Square*, 2023, https://doi.org/10.21203/rs.3.rs-2992166/v1.

[3] J. M. D'Souza, A. Bondada, and V. G. Nair, "Design and Optimization of Drone Assisted Wildfire Fighting System," *International Journal of Intelligent Engineering and Systems*, vol. 6, no. 5, pp. 2338-2348, 2025, https://doi.org/10.18196/jrc.v6i5.26058.

[4] A. Ramadhanu, R. A. Mahessya, "Development of Identification Methods Based on Soil Imagery Characteristics, Textures, and Shapes Suitable for Planting Food Crops," *International Journal of Intelligent Systems and Applications in Engineering*, vol. 11, no. 3, pp. 825-832, 2023, https://ijisae.org/index.php/IJISAE/article/view/3289.

[5] L. Liu, C. Ke, and H. Lin, "Dark-Center Based Insulator Detection Method in Foggy Environment," *Applied Sciences*, vol. 13, no. 12, p. 7264, 2023, https://doi.org/10.3390/app13127264.

[6] B. -Y. Zhang, Q. -C. Zhang and W. -Y. Zhang, "Non-Uniform Low-Light Face Image Enhancement Based on Dark Channel Prior and Image Uniform Posterior," *IEEE Access*, vol. 12, pp. 85724-85734, 2024, https://doi.org/10.1109/ACCESS.2024.3416130.

[7] M. M. Malik *et al*., "A novel deep CNN model with entropy coded sine cosine for corn disease classification," *Journal of King Saud University - Computer and Information Sciences*, vol. 36, no. 7, p. 102126, 2024, https://doi.org/10.1016/j.jksuci.2024.102126.

[8] R. Lee and C. Wong, "Single Image Integrated Deblurring Algorithm in Non-Uniform Environment," *Journal of Advanced Research in Applied Sciences and Engineering Technology*, vol. 45, no. 1, pp. 60-70, 2025, https://doi.org/10.37934/araset.45.1.6070.

[9] S. Liu, Y. Li, H. Li, B. Wang, Y. Wu, and Z. Zhang, "Visual Image Dehazing Using Polarimetric Atmospheric Light Estimation," *Applied Sciences*, vol. 13, no. 19, p. 10909, 2023, https://doi.org/10.3390/app131910909.

[10] K. J. Hu, M. Y. Chen, Y. S. Chang, and S. L. Kao, "Enhanced Color Sensing and Recognition of Underwater Color Using Robust Adaptive Tone Mapping," *Sensors and Materials*, vol. 35, no. 11, pp. 3671-3686, 2023, https://doi.org/10.18494/SAM4642.

[11] N. M. Salman, H. G. Daway, and J. A. Jouda, "Retinal image enhancement using dark channel prior," *Journal of Optics*, 2024, https://doi.org/10.1007/s12596-024-02208-y.

[12] E. Tian and J. Kim, "Improved Vehicle Detection Using Weather Classification and Faster R-CNN with Dark Channel Prior," *Electronics*, vol. 12, no. 14, p. 3022, 2023, https://doi.org/10.3390/electronics12143022.

[13] S.-H. Hwang, S.-K. Park, S.-H. Park, K.-W. Kwon, and T.-H. Im, "RDCP: A Real Time Sea Fog Intensity and Visibility Estimation Algorithm," *Journal of Marine Science and Engineering*, vol. 12, no. 1, p. 53, 2023, https://doi.org/10.3390/jmse12010053.

[14] H. Zhang, P. Lu, T. Qi, Y. Xu and T. Zeng, "Adaptive Superpixel-Guided Non-Homogeneous Image Dehazing," *IEEE Signal Processing Letters*, vol. 32, pp. 591-595, 2025, https://doi.org/10.1109/LSP.2025.3527197.

[15] G. Miao, Z. Zhang, and Z. Wang, "Analysis of the Generalization Ability of Defogging Algorithms on RICE Remote Sensing Images," *Sensors*, vol. 24, no. 14, p. 4566, 2024, https://doi.org/10.3390/s24144566.

[16] A. Khmag, "Smoke Removal Method of Industrial Images Based on Dark Channel Prior Approach and Second-Generation Wavelets," *SN Computer Science*, vol. 5, no. 843, pp. 1–10, 2024, https://doi.org/10.1007/s42979-024-03217-1.

[17] F. Ibrahim and M. S. M. Rahim, "Current Issues on Single Image Dehazing Method," *International Journal of Computer Engineering and Research Trends*, vol. 5, no. 2, pp. 37-49, 2018, https://ijcert.org/ems/ijcert_papers/V5I205.pdf.

[18] F. Liu, J. Wang, and Y. Pan, "Optimization and Performance Comparison of AOD-Net and DehazeFormer Dehazing Algorithms," *AI*, vol. 6, no. 8, p. 181, 2025, https://doi.org/10.3390/ai6080181.

[19] L. Han, H. Lv, C. Han, Y. Zhao, Q. Han, and H. Liu, "Atmospheric scattering model and dark channel prior constraint network for environmental monitoring under hazy conditions," *Journal of Environmental Sciences*, vol. 152, pp. 203-218, 2025, https://doi.org/10.1016/j.jes.2024.04.037.

[20] H. Huang, Z. Li, M. Niu, M. S. Miah, T. Gao, and H. Wang, "A Sea Fog Image Defogging Method Based on the Improved Convex Optimization Model," *Journal of Marine Science and Engineering*, vol. 11, no. 9, p. 1775, 2023, https://doi.org/10.3390/jmse11091775.

[21] H. Suo *et al*., "Dynamic Dark Channel Prior Dehazing with Polarization," *Applied Sciences*, vol. 13, no. 18, p. 10475, 2023, https://doi.org/10.3390/app131810475.

[22] K. J. Hu, Y. T. Pan, L. W. Jiang, S. Der Lee, and S. L. Kao, "A robust underwater image enhancement algorithm," *The Journal of Supercomputing*, vol. 81, no. 244, 2025, https://doi.org/10.1007/s11227-024-06719-0.

[23] C. Gong and B. Qian, "An Adaptive Brightness Global Digital Image Correlation Method for Deformation Measurement Using Overexposed Images," *Optics and Lasers in Engineering*, vol. 25, no. 13, p. 3957, 2025, https://doi.org/10.3390/s25133957.

[24] P. Kilcullen, T. Ozaki, and J. Liang, "Compressed ultrahigh-speed single-pixel imaging by swept aggregate patterns," *Nature Communications*, vol. 13, no. 1, pp. 1-10, 2022, https://doi.org/10.1038/s41467-022-35585-8.

[25] R. A. Malik, Yuhandri, and A. Ramadhanu, "Rethinking the Patch: A Dynamic Superpixel Approach for Suppressing Halo Artifacts in Dark Channel Prior Dehazing," *2025 International Conference on Information Technology Research and Innovation (ICITRI)*, pp. 1-6, 2025, https://doi.org/10.1109/ICITRI67507.2025.11232955.

[26] J. Thomas and E. D. Raj, "Improved image dehazing model with color correction transform-based dark channel prior," *The Visual Computer*, vol. 40, no. 12, pp. 8767-8790, 2024, https://doi.org/10.1007/s00371-024-03270-0.

[27] K. A. Noman and A. S. Yaseen, "Underwater image enhancement by dark channel prior," *Digital Technologies and Applications*, pp. 307-315, 2024, https://doi.org/10.1007/978-3-031-68653-5_30.

[28] G. Yang, H. Yang, S. Yu, J. Wang, and Z. Nie, "A Multi-Scale Dehazing Network with Dark Channel Priors," *Sensors*, vol. 23, no. 13, p. 5980, 2023, https://doi.org/10.3390/s23135980.

[29] H. S. Lee, S. W. Moon, I. K. Eom, "Underwater Image Enhancement Using Successive Color Correction and Superpixel Dark Channel Prior," *Symmetry*, vol. 12, no. 8, p. 1220, 2020, https://doi.org/10.3390/sym12081220.

[30] A. S. P and J. EP, "Fusion of near-infrared and visible light images under hazy environment using multiplicative dark channel prior," *Multimedia Tools and Applications*, vol. 84, pp. 5287-5310, 2024, https://doi.org/10.1007/s11042-024-18995-2.

[31] K. Hu, Q. Zeng, J. Wang, J. Huang, and Q. Yuan, "A Method for Defogging Sea Fog Images by Integrating Dark Channel Prior with Adaptive Sky Region Segmentation," *Journal of Marine Science and Engineering*, vol. 12, no. 8, p. 1255, 2024, https://doi.org/10.3390/jmse12081255.

[32] V. N. More and V. Vyas, "Removal of fog from hazy images and their restoration," *Journal of King Saud University - Engineering Sciences*, vol. 3, no. 8, pp. 600-610, 2022, https://doi.org/10.1016/j.jksues.2022.01.002.

[33] C. Hao, Y. He, Y. Li, X. Niu, and Y. Wang, "A fast specular removal method for a single real image," *Displays*, vol. 87, p. 102930, 2025, 2024, https://doi.org/10.1016/j.displa.2024.102930.

[34] L. Zou, Y. Zheng, and J. Lu, "An Edge Detection Method for Welding Pool Based on An Improved Canny Algorithm," *Journal of Physics: Conference Series*, vol. 2785, no. 1, 2024, https://doi.org/10.1088/1742-6596/2785/1/012013.

[35] N. A. Khalaf, H. G. Daway, and B. M. Ahmed, "Aerial Images Enhancement Using Perceptual Dark Channel Prior," *International Journal of Intelligent Engineering and Systems*, vol. 16, no. 3, pp. 302-309, 2023, https://doi.org/10.22266/ijies2023.0630.24.

[36] S. Munaf, A. Bharathi, and A. N. Jayanthi, "FPGA-based low-light image enhancement using Retinex algorithm and coarse-grained reconfigurable architecture," *Scientific Reports*, vol. 14, no. 1, pp. 1-19, 2024, https://doi.org/10.1038/s41598-024-80339-9.

[37] J. Raninen, L. Zhu, and E. Hattula, "Study on the effect of color space in deep multitask learning neural networks for road segmentation," *ISPRS Annals of the Photogrammetry, Remote Sensing and Spatial Information Sciences*, vol. 10, pp. 201-208, 2024, https://doi.org/10.5194/isprs-annals-X-4-W4-2024-201-2024.

[38] Y. -W. Chen and S. -C. Pei, "Always Clear Days: Degradation Type and Severity Aware All-in-One Adverse Weather Removal," *IEEE Access*, vol. 13, pp. 7650-7662, 2025, https://doi.org/10.1109/ACCESS.2025.3526168.

[39] Y. Xu, "An Adaptive Dehazing Network based on Dark Channel Prior and Image Segmentation," *Journal of Physics: Conference Series*, vol. 2646, no. 1, p. 012009, 2023, https://doi.org/10.1088/1742-6596/2646/1/012009.

[40] X. Wang, B. Yuan, H. Dong, Q. Hao, and Z. Li, "End-to-End Multi-Scale Adaptive Remote Sensing Image Dehazing Network," *Sensors*, vol. 25, no. 1, p. 218, 2025, https://doi.org/10.3390/s25010218.

[41] S. Anan, M. I. Khan, M. M. S. Kowsar, K. Deb, P. K. Dhar, and T. Koshiba, "Image Defogging Framework Using Segmentation and the Dark Channel Prior," *Entropy*, vol. 23, no. 3, p. 285, 2021, https://doi.org/10.3390/e23030285.

[42] M. Mukaida, T. Koga, and N. Suetake, "Visibility improvement of hazy images using manipulation of convex combination coefficients of equi-hue planes' vertices in the RGB color space," *Signal, Image and Video Processing*, vol. 19, no. 53, 2025, https://doi.org/10.1007/s11760-024-03578-3.

[43] R. Qasrawi *et al*., "Hybrid ensemble deep learning model for advancing breast cancer detection and classification in clinical applications," *Heliyon*, vol. 10, no. 19, p. e38374, 2024, https://doi.org/10.1016/j.heliyon.2024.e38374.

[44] B. Liang, Y. Tao, Y. Song, and X. Li, "An Image Restoration Method for Improving Matching Robustness of Indoor Smoke Scene," *Fire Technology*, vol. 61, no. 2, pp. 483-511, 2024, https://doi.org/10.1007/s10694-024-01623-8.

[45] R. M. Habeeb, M. H. Mohammed, H. G. Daway, H. H. kareem, and G. Z. Alwan, "Enhancement X-ray image using modified dark channel prior based on Otsu segmentation," *Journal of Optics*, vol. 54, pp. 3554-3563, 2024, https://doi.org/10.1007/s12596-024-01977-w.

[46] J. Lu *et al*., "MSIMRS: Multi-Scale Superpixel Segmentation Integrating Multi-Source Remote Sensing Data for Lithology Identification in Semi-Arid Area," *Remote Sensing*, vol. 17, no. 3, p. 387, 2025, https://doi.org/10.3390/rs17030387.

[47] R. A. Malik, Yuhandri and A. Ramadhanu, "A Unified Dehazing Framework: Synergizing CLAHE and Dark Channel Prior in YCbCr Space to Optimize Quality and Latency," *2025 International Conference on Information Technology Research and Innovation (ICITRI)*, pp. 1-6, 2025, https://doi.org/10.1109/ICITRI67507.2025.11232680.

[48] C. Li *et al*., "Single-Image Dehazing Based on Improved Bright Channel Prior and Dark Channel Prior," *Electronics*, vol. 12, no. 2, p. 299, 2023, https://doi.org/10.3390/electronics12020299.

[49] X. Wu *et al*., "A real-time framework for HD video defogging using modified dark channel prior," *Journal of Real-Time Image Processing*, vol. 21, no. 55, pp. 1-15, 2024, https://doi.org/10.1007/s11554-024-01432-w.

[50] Y. Xu, H. Zhang, F. He, J. Guo, and Z. Wang, "Enhanced CycleGAN Network with Adaptive Dark Channel Prior for Unpaired Single-Image Dehazing," *Entropy*, vol. 25, no. 6, p. 856, 2023, https://doi.org/10.3390/e25060856.

[51] W. Yu, "Image processing methods based on physical models," *Results in Physics*, vol. 56, p. 107199, 2024, https://doi.org/10.1016/j.rinp.2023.107199.

[52] S. K. Kuanar, R. Panda, and A. S. Chowdhury, "Video key frame extraction through dynamic Delaunay clustering with a structural constraint," *Journal of Visual Communication and Image Representation*, vol. 24, no. 7, pp. 1212-1227, 2013, https://doi.org/10.1016/j.jvcir.2013.08.003.

[53] Y. Han and Y. Liu, "Intelligent Classification and Segmentation of Sandstone Thin Section Image Using a Semi-Supervised Framework and GL-SLIC," *Minerals*, vol. 14, no. 8, p. 799, 2024, https://doi.org/10.3390/min14080799.

[54] J. -F. Song, H. -L. Zhao, D. -Y. Wen and X. -Y. Xu, "Video Anomaly Detection Based on Optical Flow Feature Enhanced Spatio–Temporal Feature Network FusionNet-LSTM-G," *IEEE Access*, vol. 10, pp. 130314-130325, 2022, https://doi.org/10.1109/ACCESS.2022.3229420.

[55] Q. Gao *et al*., "Improved adaptive FPGA dark channel prior dehazing algorithm for edge applications in agricultural scenarios," *Smart Agricultural Technology*, vol. 12, p. 101285, 2025, https://doi.org/10.1016/j.atech.2025.101285.

[56] L. Wu *et al*., "Hybrid Dark Channel Prior for Image Dehazing Based on Transmittance Estimation by Variant Genetic Algorithm," *Applied Sciences*, vol. 13, no. 8, p. 4825, 2023, https://doi.org/10.3390/app13084825.

[57] L. A. Tran, D. Kwon, and D. C. Park, "Single Image Dehazing via Regional Saturation-Value Translation," *Procedia Computer Science*, vol. 237, pp. 517-524, 2024, https://doi.org/10.1016/j.procs.2024.05.135.

[58] S. Liu, P. Chen, J. Lan, J. Li, Z. Shen, and Z. Wang, "Underwater image restoration via multiscale optical attenuation compensation and adaptive dark channel dehazing," *Computers & Electrical Engineering*, vol. 123, p. 110228, 2025, https://doi.org/10.1016/j.compeleceng.2025.110228

[59] P. Sun *et al*., "Virtual cleaning of sooty mural hyperspectral images using the LIME model and improved dark channel prior," *Scientific Reports*, vol. 14, no. 1, pp. 1-20, 2024, https://doi.org/10.1038/s41598-024-75801-7.

[60] S. Lee, S. Yun, J. H. Nam, C. S. Won, and S. W. Jung, "A review on dark channel prior based image dehazing algorithms," *EURASIP Journal on Image and Video Processing*, vol. 2016, no. 4, pp. 1-23, 2016, https://doi.org/10.1186/s13640-016-0104-y.

[61] V. Baldeva, V. Sharma, S. Verma, P. Kansal, S. Kansal, and J. Narayan, "Pixel-Dehaze: Deciphering Dehazing Through Regression-Based Depth and Scattering Estimation," *The Visual Computer*, vol. 9, no. 11, p. 282, 2025, https://doi.org/10.3390/bdcc9110282.

[62] J. B. Mohapatra, N. K. Nishchal, and J. Monikantan, "Object Recognition in Foggy and Hazy Conditions Using Dark Channel Prior-Based Fringe-Adjusted Joint Transform Correlator," *Photonics*, vol. 11, no. 12, p. 1142, 2024, https://doi.org/10.3390/photonics11121142.

[63] P. Li, D. Qiao, C. Luo, D. Wan, and G. Li, "Hybrid Regularized Variational Minimization Method to Promote Visual Perception for Intelligent Surface Vehicles Under Hazy Weather Condition," *Journal of Marine Science and Engineering*, vol. 13, no. 10, p. 1991, 2025, https://doi.org/10.3390/jmse13101991.

[64] D. Zhang, G. Sun, Z. Yang, and J. Yu, "A high-density gamma white spots-Gaussian mixture noise removal method for neutron images denoising based on Swin Transformer UNet and Monte Carlo calculation," *Nuclear Engineering and Technology*, vol. 56, no. 2, pp. 715-727, 2024, https://doi.org/10.1016/j.net.2023.11.011.

[65] S. Wang, M. Zhang, "Atmospheric Scattering Prior Embedded Diffusion Model for Remote Sensing Image Dehazing," *Atmosphere*, vol. 16, no. 9, p. 1065, 2025, https://doi.org/10.3390/atmos16091065.

[66] Y. Liu, X. Wang, L. Sun, J. Chen, J. He, and Y. Zho, "Shallow Marine High-Resolution Optical Mosaics Based on Underwater Scooter-Borne Camera," *Sensors*, vol. 23, no. 19, p. 8028, 2023, https://doi.org/10.3390/s23198028.

[67] A. More and S. Lahudkar, "Analysis and Synthesis of Image Dehazing Using Deep Learning Algorithm," *International Journal of Intelligent Systems and Applications in Engineering*, vol. 12, no. 12s, pp. 121-128, 2024, https://ijisae.org/index.php/IJISAE/article/view/4496.

[68] H. Gang *et al*., "Single image dehazing algorithm using complementary saturation prior," *Signal, Image and Video Processing*, vol. 19, no. 224, pp. 1-10, 2025, https://doi.org/10.1007/s11760-024-03782-1.

[69] Q. Chen, H. Liu, and W. Gan, "A real-time recognition and distance measurement method for underwater dynamic obstacles based on binocular vision," *Measurement*, vol. 252, p. 117329, 2025, https://doi.org/10.1016/j.measurement.2025.117329.